# Dam leakage detection based on unmanned aerial vehicle multi-sensor

Tongqi Wang<sup>1</sup>,Shan Su<sup>1</sup>,Changjun Chen<sup>1,2\*</sup>

Wuhan University, School of Geodesy and Geomatics, Wuhan 430079, China - wangtongqi@whu.edu.cn(T.W.);sushan@whu.edu.cn (S.S.)
Hubei Luojia Laboratory, Wuhan 430079, China
\* Correspondence : chencj@whu.edu.cn(C.C.)

Keywords: Dam leakage; Image processing; UAV surveying and mapping; Multi sensor; Disaster Emergency Management

### **Abstract**

In response to the problems of low efficiency, high cost, single data type, and potential safety hazards existing in traditional dam leakage detection methods, this study integrates sensors such as thermal infrared cameras, RGB cameras, and LiDAR into lightweight unmanned aerial vehicles to construct a multi sensor integrated system. This system can acquire multi source data of dam structures and their surrounding environments in real time, rapidly, all day long, comprehensively, and non contact. In the data processing stage, the thermal infrared images are first enhanced to improve the image quality, and the multi source data registration is completed. Subsequently, the Hierarchical Context Fusion Network is used, combined with information such as point cloud intensity and river water height, to identify potential leakage areas. Then, the Density Based Spatial Clustering of Applications with Noise algorithm is utilized to optimize the results, and the RGB images are used as an aid to accurately locate the leakage points. By processing the data collected from a certain dam, the reliability of the multi sensor equipment and the multi level suspected hazard detection algorithm is verified. This application can reliably detect and locate suspected hazards, significantly reduce the time and resource costs of dam detection, and simultaneously reduce the safety risks of dam detection personnel.

#### 1. Introduction

As an inaccessible part of the flood control system, river embankments are an important guarantee for social production and people's lives. However, leakage is one of the most common and harmful diseases in earth-rock embankments, often occurring during the flood season. If the leakage of the embankment is not discovered and dealt with in time, it is easy to cause the river embankment to burst, endangering the life and property safety of the surrounding residents.

Traditionally, weirs and pressure gauges have been placed at critical points in the embankment to monitor seepage and leakage. However, the coverage of this monitoring method is very limited, and it is a point monitoring, which can only cover a few key parts. The development of non-destructive testing techniques such as ground penetrating radar, high-density resistivity and transient electromagnetic has greatly improved the scope and efficiency of dike leak diagnosis. However, the process of interpreting the data obtained by these NDT methods is quite complex, resulting in inefficiency and high cost. The distributed fiber optic temperature monitoring system has the advantages of good time continuity and wide spatial coverage. However, this method requires fibre to be buried in the embankment in advance, which is not practical for an already built embankment.

At present, manual dike inspection is still the main means to detect dike leakage during the flood season. On the one hand, this method consumes a lot of manpower and financial resources, and because it is the flood season, heavy rains are frequent, and the personal safety of inspectors is also at risk. On the other hand, due to the limitations of observation and range of motion, it is often impossible to detect existing leakage areas. Especially at night, the observation efficiency and patrol range will be greatly reduced. Therefore, it is an urgent task to study efficient dam data collection and leakage identification methods.

In general, the shape of the embankment is linear, and its length is usually several kilometers or even tens of kilometers. Drones with integrated non-contact sensors are ideally suited to monitor such extra long linear structures. Currently, certain achievements have been made in the research of using drones equipped with multi-sensors to detect dam leakage.(Li et al., 2023) achieved the automatic identification of piping hazards in earth rock embankments of small and medium sized rivers based on UAV thermal infrared and visible light images. (Su et al.,2022) detected and identified earth rock dam leakage by means of UAV visible and infrared images. (Zhou et al.,2022) accomplished the automatic recognition of earth rock dam leakage by applying UAV passive infrared thermography combined with deep learning technology. (Zhou et al.,2024) successfully realized the automatic localization of dam leakage outlets using UAV thermography and YOLO - based object detectors.

However, due to the presence of vegetation cover, complex textures, and uneven lighting on the surface of the dam, when relying solely on infrared and visible light images for detection, a large number of misidentifications often occur. For example, the characteristics of vegetation may be similar to those of the leakage area, leading to misjudgments. Complex lighting conditions can affect the image quality and interfere with the extraction of leakage features.

Inspired by the multi - level detection approach proposed in (Su et al.,2024) , we utilize a lightweight drone equipped with a thermal infrared imager, a visible light camera, a LiDAR, and other sensors to collect data comprehensively. This enables us to obtain a more complete set of information about the dam and its surrounding environment., we use a light drone equipped with thermal infrared imager, visible light camera, lidar and other sensors to realize data collection, and design a set of multi-level dam leakage identification algorithm based on multi-source data to achieve accurate detection of the dam leakage area.

#### 2. Materials

The multi-sensor system constructed in this study is integrated into the UAV platform. It consists of a Global Navigation Satellite System (GNSS) positioning and orientation system, a CHC Navigation AlphaAir 450 pocket LiDAR, a FLIR VUE Pro R thermal infrared camera, and an RGB camera built into the AlphaAir 450 LiDAR system, which work together to provide comprehensive data support for levee detection(see Figure 1, Figure 2, Figure 3, Figure 4).



Figure 1. CHCNAV's emergency intelligent patrol AR-10.



Figure 2. AlphaAir 450 pocket LiDAR



Figure 3. FLIR VUE Pro R camera



Figure 4. CHCNAV's quadcopter UAV

The FLIR Vue Pro R is a thermal imaging camera for small drones that uses the long-wave infrared band (7.5-13  $\mu m$ ) to observe objects on the ground. The instrument acquires accurate, non-contact temperature measurement data and embeds calibrated temperature information into every pixel. Table 1 details the characteristics of the FLIR Vue Pro R camera.

FLIR Vue Pro R camera	
Focal length	19 mm
FoV	32° × 26°
Image resolution	640 × 512 pix
Spectral band	7.5-13.5 μm

Table 1. Characteristics of the FLIR Vue Pro R camera.

Lidar measures the distance from the target to the receiver by emitting a laser beam to obtain accurate 3D point cloud data. Based on the design concept of lightweight and high integration, we chose the CHC navigation AlphaAir 450 pocket lidar. The radar has a built-in camera, and the entire payload weighs only 950g, enabling high-precision, high-density, and efficient real-time data acquisition, and its characteristics are detailed in Table 2.

CHC navigation AlphaAir 450 pocket lidar	
Weight	950 g
FoV	75°
Ranging Accuracy	1.5cm
Ranging	5-480m
Point Frequency	0.3 million points/s

Table 2. Characteristics of CHC navigation AlphaAir 450 pocket lidar

RGB cameras capture visible light reflected from the surface of an object while imaging, and the quality of the image is affected by the object's reflectivity and external illumination intensity. The image information has low requirements for the professional knowledge of the embankment patrol personnel, and can be used as an auxiliary judgment basis. The AlphaAir 450 LiDAR system has a built-in 24MP camera capable of generating digital orthophoto maps (DOMs), digital surface models (DSMs), and color point clouds, and the RGB camera's specifications are detailed in Table 3.

RGB camera	
Resolution	6252×4168
Field of View	72.5° × 52.2°
The Minimum	1s
Photographing Interval	18
Focal Length	16mm

Table 3. The technical parameters of the RGB camera.

The multi-sensor integration we have developed is a stand-alone system that can be mounted on a drone platform. In this study, the device was deployed on the CHCNAV's quadcopter UAV platform. The technical specifications of the drone platform are detailed in Table 4.

CHCNAV's quadcopter UAV	
Size	$770 \times 804 \times 450 \text{ mm}$
Payload Weight	5kg
Maximum Takeoff Weight	13.9kg
Single-flight Range	>5km
Flight Duration	Operating time with AlphaAir 450 mounted: 52 min; Empty load operation: 58 min

Table 4. The technical parameters of the CHCNAV's quadcopter UAV.

The unified time reference requires that the acquisition system has absolute time accuracy within a specific error range and enables ultra low latency synchronous data acquisition of multiple sensors. In practical applications, the precise alignment of multi-source data has been completed in the AA450 system.

#### 3. Method

## 3.1 Infrared image enhancement

In the original thermal infrared image, the low temperature object has a low gray value and a dark tone. During preprocessing, in order to facilitate dataset production and object detection, the image pixels are inversely transformed, and the gray value of each pixel is subtracted by 255 to brighten the low-temperature object.

In addition, due to the characteristics of the detection component of the thermal infrared camera and the temperature distribution of the surface of the object, the gray scale changes obviously when the ground temperature of the thermal infrared image changes greatly, resulting in low image contrast, unclear target edges, and aggravated blur when the drone moves quickly. In order to use the temperature distribution profile and gray gradient to screen the hidden danger area, the contrast stretching enhancement image was used in the preprocessing stage to make the gray value cover the range of 0 to 255, so as to improve the contrast between the background and the target, and improve the efficiency and accuracy of the detection of the hidden danger of the embankment. The stretched pixel value can be calculated using the following formula:

$$I(x,y)_{s} = \frac{(I(x,y) - I_{min}) \times 255}{I_{max} - I_{min}}$$
(1)

### 3.2 Multi-level hazard detection

In order to realize the efficient use of multi-source data collected by UAVs and the accurate identification of leakage areas, a set of multi-level dike leakage identification algorithms based on multi-source data was constructed in this study. The algorithm can effectively identify dangerous areas that are difficult to detect with the naked eye, and provide strong

support for the safety of embankment projects. The framework is illustrated in Figure 5.

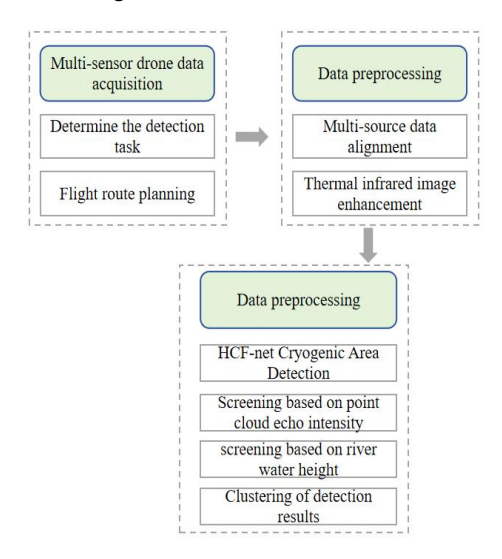


Figure 5. Workflow for Dam Leakage Inspection.

In water conservancy engineering, the specific heat capacity of water is about  $4.2 \times 10^3 \text{J/(kg} \cdot ^{\circ}\text{C)}$ , while that of soil and rock media is mostly in the range of  $0.8 \times 10^3 \text{J/(kg} \cdot ^{\circ}\text{C)} - 1.2 \times 10^3 \text{J/(kg} \cdot ^{\circ}\text{C)}$ , showing a significant difference. During solar radiation, the temperature changes of the two are different, resulting in the difference between the water temperature of the river and the water temperature of the embankment slope and the foot of the slope. In this way, thermal anomalies can be used to indirectly detect dike leakage.

Inspired by the infrared small target detection algorithm, this paper uses the Hierarchical Context Fusion Network (HCFnet) to preliminarily identify the hidden dangers of the embankment based on the enhanced thermal infrared image (Xu et al., 2024). HCF-Net is based on an upgraded U-Net architecture consisting of an encoder, decoder, and middle layer. The encoder is responsible for feature extraction and downsampling, including the Parallel Patch Perceived Attention (PPA) module and the maximum pooling layer. The decoder is used for upsampling and feature reconstruction and consists of a PPA module and a transposed convolutional (CT) layer. In the middle layer, a Multi-Expansion Channel Refiner (MDCR) module is introduced to connect codecs and enhance feature fusion. The hop-on connection component is integrated into the Dimension-Aware Selective Integration (DASI) module to promote feature fusion and propagation, and improve the detection effect of infrared small targets.

When detecting suspected hazardous areas, it is of crucial importance to distinguish between water bodies and other terrains. Due to the weak reflection of laser beams by pure water, the point cloud echo intensity is close to zero, and there is usually a continuous flow of water in the area where leakage occurs. Specifically, we first calculate the average point cloud echo intensity values of the corresponding areas in the point cloud image using the acquired mask region, and arrange them in ascending order of average echo intensity. During this process, areas with values less than 10 are filtered out. Since the echo intensity of pure water points is close to zero, it can be used to distinguish water bodies from other terrains. The lower the value, the higher the water content, and the higher the risk

level of the suspected hazardous area, which requires manual emergency investigation.

Analyzing from the principle of leakage, leakage occurs due to the presence of pressure differences and permeable channels. River water penetrates into other areas through these channels under pressure. Above the river surface, there is no pressure to drive the river water, and thus there is no main power source for water infiltration. Even if there are some minor defects in the embankment, it is difficult to form significant leakage without external water pressure. Therefore, after obtaining the river water level through the point cloud information, the potential hazards in the suspected hazardous areas above the river water level can be excluded, thereby improving the detection accuracy.

The results obtained through multi level detection are often discrete, with noise and small areas that may be misidentified. In order to better analyze and process these results, this paper uses the DBSCAN clustering algorithm to process the identification results. Based on the principle of data point density, this algorithm can divide the density - connected data points in space into different clusters by setting two key parameters: neighborhood radius (eps) and minimum number of points (MinPts). Among them, points that contain a number of data points greater than or equal to the minimum number of MinPts within the neighborhood radius eps are marked as core points. The core points and their density connected points form clusters. Points that fall within the neighborhood of core points but are not core points themselves are boundary points, and the rest are noise points.

### 4. Results

As June is the flood season in Hunan, frequent heavy rainfall causes a sharp rise in river water levels, and the risk of dam leakage increases dramatically. To verify the reliability of the algorithm, this paper applies the proposed algorithm to a set of dam data collected in Hunan in June 2023.

# 4.1 Infrared Image Enhancement

In the dam area, the surrounding environment is generally covered by a large area of vegetation, bare soil, and diverse terrains. In addition, due to the relatively limited field of view of the infrared thermal imager, there are a large number of repetitive landscapes in the captured scenes. Affected by these factors, the thermal infrared images are blurry, the terrain contours are unclear, and the image contrast is significantly reduced.In this study, a contrast stretching algorithm was used to enhance the thermal infrared images. Considering the requirements of infrared small target detection, the infrared images were first subjected to grayscale inversion, and then the inverted images were enhanced. As can be seen from Figure 3, the clarity of the terrain contours in the enhanced thermal infrared images has been significantly improved, and the contrast between the terrain areas corresponding to different radiation temperatures has also been significantly enhanced.







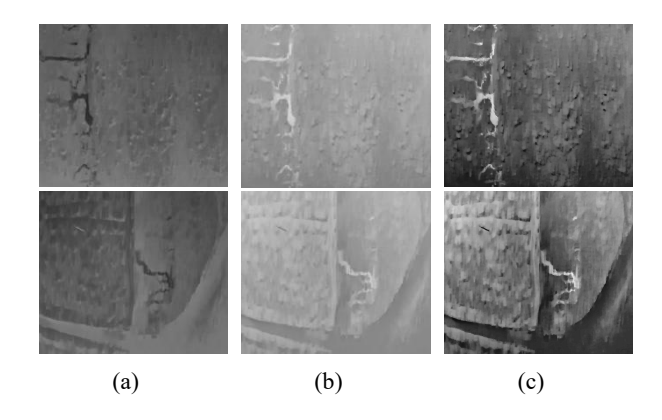


Figure 6. Thermal infrared image enhancement results. (a)original thermal infrared image,(b)inverted thermal infrared image,(c)enhanced thermal infrared image.

### 4.2 Multi-level Detection of Dam Leakage

Since the targets to be detected have no fixed constraints such as shape and size, and there is a lack of publicly available datasets, we utilized experimental test data and on site data from other dams as the training set and the test set. In total, these data contain 207 thermal infrared images. Among them, the training set and the test set account for 70% and 30% of the total number of images respectively.

During the manual annotation stage, we first used the images that had undergone morphological gradient edge detection as a reference, and then used the Labelme software to create labels on the infrared images. Specifically, this process first identified the regions with significant gradient changes in the thermal infrared images, with a particular focus on recognizing the low-temperature regions. This method ensures more accurate annotation of the targets.

Since the target areas in the dam thermal infrared images we need to process vary greatly in shape and size, lack clear and fixed features, and the images are blurred with low contrast, the target detection task is extremely challenging. We use a combined loss function to train the network, specifically by combining Binary Cross Entropy Loss (Bce-loss) and Intersection over Union Loss (Iou-loss), with the weights of both set to 1. Meanwhile, the AdamW method is used for optimization, and the CosineAnnealingLR scheduler is employed to adjust the learning rate. The initial learning rate is set to 0.0005, the total number of training epochs is 1000, and the batch size is 4. To evaluate the network performance, we adopt the Intersection over Union (IoU) as evaluation metrics.

$$IoU = \frac{|A \cap B|}{|A \cup B|} \tag{2}$$

Among them,A is the region corresponding to the prediction box (Prediction Box), and B is the region corresponding to the ground truth box (Ground Truth Box).IoU is used to measure the overlapping degree between the prediction result and the ground truth annotation, which is obtained by calculating the ratio of the intersection area to the union area of the predicted bounding box and the ground truth bounding box.The final trained network achieved an IoU of 79.26%.

In the designed algorithm, we first send the enhanced thermal infrared image to the trained infrared small target detection network for temperature anomaly area recognition, which effectively screens out all the high-temperature areas in the target area before image preprocessing. Preliminary examination marked 172 thermal infrared images of possible pipe surges.

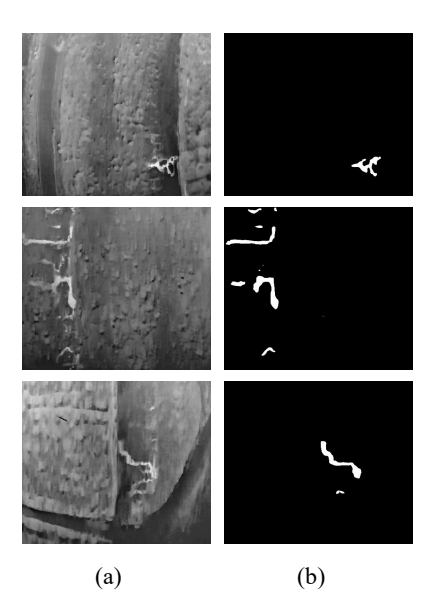
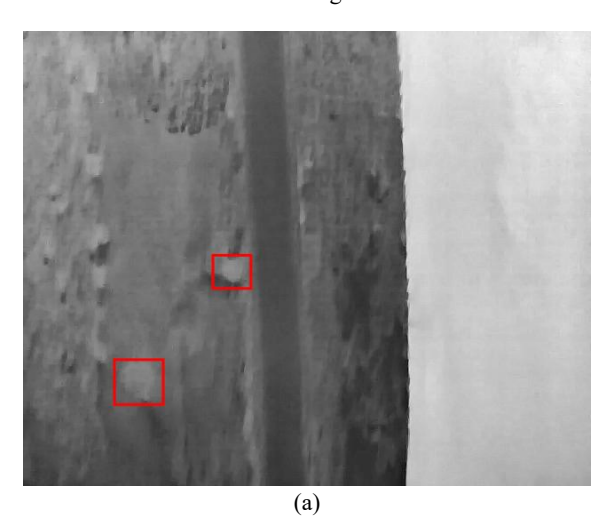


Figure 7. HCF-net screening results for low-temperature regions. (a)enhanced thermal infrared image,(b)the low-temperature regions detected by the HCF-net.

Areas covered by vegetation usually also exhibit temperature anomaly phenomena. The reflectivity of water bodies to laser is approximately 2% - 5%, while the reflectivity of vegetation to near - infrared band lasers generally ranges from 10% to 30%. This difference is reflected in the point cloud intensity. Therefore, this study introduces the analysis of the point cloud intensity of suspicious areas to improve the accuracy of the detection results. In practical applications, we calculate the average point cloud intensity for each area, and determine whether to retain the area according to the set threshold.



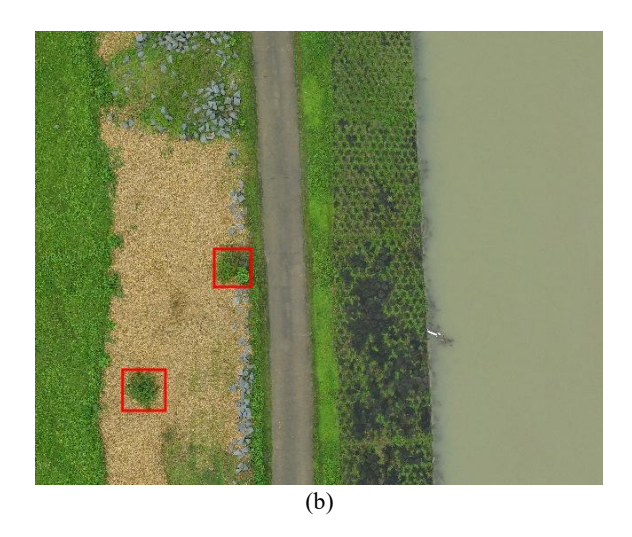


Figure 8 Thermal infrared image of areas containing vegetation. (a)enhanced thermal infrared image,(b)visible light image.

Since dam leakage occurs when river water is driven by a pressure difference, areas above the river water level have no water pressure acting on them. By determining the height of the river water, we excluded some of the suspicious areas located above the river water level.

The results obtained by the above algorithms will have noise interference, and the results of the algorithms are relatively discrete when performing the recognition task. By introducing a clustering algorithm to process these results in depth, the noise points can be accurately identified and removed, and the leakage information belonging to the same area can be effectively integrated.

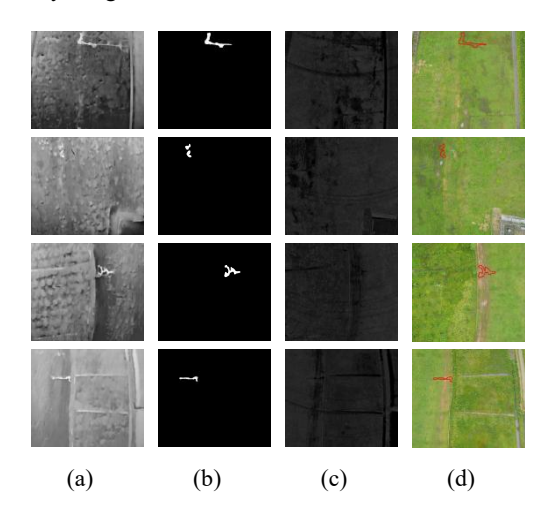


Figure 9. Results of multi-level dam detection. (a)enhanced thermal infrared image,(b)mask image of low-temperature areas,(c)point cloud intensity image,(d)visible light image projected with dangerous areas.

After the above multi-level detection process, 18 potentially risky areas were obtained. Considering the flight speed of the unmanned aerial vehicle and the image capture frequency, there is inevitably redundancy in the data. After obtaining the geographical locations of the suspicious areas, only 4 areas were determined to have dam leakage.

#### 5. Conclusions

This study focuses on the problems of low efficiency, high cost, single data type, and potential safety hazards in traditional dam leakage detection. A multi-sensor integrated system for lightweight unmanned aerial vehicles (UAVs) was constructed, integrating multiple sensors such as thermal infrared cameras, RGB cameras, and LiDAR. This system enables the efficient collection of multi-source data of dams and their surrounding environments during the flood season.

In the data processing stage, the thermal infrared images are first enhanced to improve the image quality, and the multisource data registration is completed simultaneously. Subsequently, the Hierarchical Context Fusion Network (HCF-Net) is used, combined with information such as point cloud intensity and river water height, to identify potential leakage areas. These results are then optimized by the Density-Based Spatial Clustering of Applications with Noise (DBSCAN) algorithm, and the RGB images are used as an aid to accurately locate the leakage points.

Through the actual detection of a dam in Hunan, four leakage areas were accurately identified based on the acquired multisource data, verifying the feasibility of this method. This method effectively improves the detection efficiency and accuracy and reduces the risks of manual detection.

In the future, there are plans to construct a large-scale dataset to optimize the model and enhance its generalization ability. Additionally, the fusion of point cloud intensity images and infrared images for training will be considered to further improve the detection accuracy.

### References

- Li, R., Wang, Z., Sun, H., Zhou, S., Liu, Y., & Liu, J. (2023). Automatic identification of earth rock embankment piping hazards in small and medium rivers based on UAV thermal infrared and visible images. Remote Sensing, 15(18), 4492.
- Su, S., Yan, L., Xie, H., Chen, C., Zhang, X., Gao, L., & Zhang, R. (2024). Multi-Level Hazard Detection Using a UAV-Mounted Multi-Sensor for Levee Inspection. Drones, 8(3), 90.
- Su, H., Ma, J., Zhou, R., & Wen, Z. (2022). Detect and identify earth rock embankment leakage based on UAV visible and infrared images. Infrared Physics & Technology,122, 104105.
- Xu, S., Zheng, S., Xu, W., Xu, R., Wang, C., Zhang, J., ... & Guo, L. (2024). HCF-Net: Hierarchical Context Fusion Network for Infrared Small Object Detection.arXiv preprint arXiv:2403.10778.
- Zhou, R., Wen, Z., & Su, H. (2022). Automatic recognition of earth rock embankment leakage based on UAV passive infrared thermography and deep learning.ISPRS Journal of Photogrammetry and Remote Sensing,191, 85-104.
- Zhou, R., Almustafa, M. K., Nehdi, M. L., & Su, H. (2024). Automated localization of dike leakage outlets using UAV-borne thermography and YOLO-based object detectors.ISPRS Journal of Photogrammetry and Remote Sensing,218, 551-573.